Received: 19 September 2021 | Revised: 12 December 2021 | Accepted: 24 January 2022

DOI: 10.1002/elps.202100304

ELECTROPHORESIS

RESEARCH ARTICLE

On-chip microfluidic buffer swap of biological samples in-line with downstream dielectrophoresis

Xuhai Huang[1] | **Karina Torres-Castro**[1] | **Walter Varhue**[1] | **Aditya Rane**[2] | **Ahmed Rasin**[1] | **Nathan S. Swami**[1,2]

[1]Electrical and Computer Engineering, University of Virginia, Charlottesville, Virginia, USA

[2]Department of Chemistry, University of Virginia, Charlottesville, Virginia, USA

Correspondence
Nathan S. Swami, Electrical and Computer Engineering, University of Virginia, Charlottesville, VA 22904, USA.
Email: nswami@virginia.edu

Xuhai Huang and Karina Torres-Castro have contributed equally.

Color online: See article online to view Figures 1–5 in color.

Funding information
NSF, Grant/Award Number: 2051652; AFOSR, Grant/Award Number: FA2386-21-1-4070; NCI Cancer Center Support, Grant/Award Number: P30 CA44579

Abstract

Microfluidic cell enrichment by dielectrophoresis, based on biophysical and electrophysiology phenotypes, requires that cells be resuspended from their physiological media into a lower conductivity buffer for enhancing force fields and enabling the dielectric contrast needed for separation. To ensure that sensitive cells are not subject to centrifugation for resuspension and spend minimal time outside of their culture media, we present an on-chip microfluidic strategy for swapping cells into media tailored for dielectrophoresis. This strategy transfers cells from physiological media into a 100-fold lower conductivity media by using tangential flows of low media conductivity at 200-fold higher flow rate versus sample flow to promote ion diffusion over the length of a straight channel architecture that maintains laminarity of the flow-focused sample and minimizes cell dispersion across streamlines. Serpentine channels are used downstream from the flow-focusing region to modulate hydrodynamic resistance of the central sample outlet versus flanking outlets that remove excess buffer, so that cell streamlines are collected in the exchanged buffer with minimal dilution in cell numbers and at flow rates that support dielectrophoresis. We envision integration of this on-chip sample preparation platform prior to or post-dielectrophoresis, in-line with on-chip monitoring of the outlet sample for metrics of media conductivity, cell velocity, cell viability, cell position, and collected cell numbers, so that the cell flow rate and streamlines can be tailored for enabling dielectrophoretic separations from heterogeneous samples.

KEYWORDS
dielectrophoresis, microfluidics, sample preparation, separation, tangential flows

1 | INTRODUCTION

Biological samples used in basic research and in clinical diagnostic settings often display a degree of heterogeneity that arises due to cellular subpopulations [1], which is

Abbreviations: DEP, dielectrophoresis; nDEP, negative dielectrophoresis; pDEP, positive dielectrophoresis; RBCs, red blood cells.

an essential feature of the hierarchical organization and functioning of biological systems. Such heterogeneity poses challenges toward correlating specific cell types and markers to functional outcomes of interest to disease onset and progression [2]. This is often addressed by using antibody receptors to surface markers that identify each cell type, for sorting cells of interest after fluorescent staining [3] or magnetic functionalization [4], but these sample preparation operations can be time consuming, require costly chemicals, introduce a degree of selection bias, and cause sample dilution to limit the enrichment level possible for fractional subpopulations. Furthermore, characteristic cellular surface markers are often not available for key biological functions, such as cancer metastasis [5], stem cell differentiation lineage [6], and immune cell activation [7]. Hence, label-free cellular separations based on their inherent biophysical properties are gaining interest, with microfluidic systems offering a dynamic platform with sufficient force fields for controlled deflection of a particular cell type from heterogeneous samples. Platforms for cell separations based on biophysical differences [8] in size [9], shape [10], deformability [11], and electrical properties [12] are particularly of great interest to quantify heterogeneity of cellular systems.

For the purposes of cell separation based on subcellular differences in physiology, such as electrical size, membrane morphology, and cytoplasmic organization, there is much interest in dielectrophoresis (DEP) [13, 14], wherein microfluidic systems can be designed with spatial field non-uniformities, for translation of polarized cells towards the high field region by positive DEP (pDEP) or for translation of cells away from the high field due to polarization of the surrounding media [15–17]. In this manner, DEP has been applied to isolate circulating tumor cells [18, 19], stem cell progenitors [20], cells based on their mitochondrial phenotype [21], bacterial strain discrimination [22, 23], and isolation of secreted exosomes [24, 25]. The DEP trapping force (F_{DEP}) for manipulating cells in a biological sample depends on the dielectric contrast between the cell and its surrounding media, at specific frequencies of the applied electric field. Other factors determining F_{DEP} include dependence on the product of the electric field (E) to its spatial non-uniformity (∇E), represented as: ∇E^2, and a cube-fold dependence on the hydrodynamic radius of the cell (a). At typical operating frequencies for DEP (<10 MHz), the dielectric contrast is chiefly determined by the difference in conductivity of the cell interior (σ_{cell}) to that of the suspending media (σ_m). Hence for biological cells that usually have an interior conductivity in the 5000–15 000 μS/cm range, significant levels of pDEP can only be observed within media of conductivity in the 100–1000 μS/cm range and under electric fields in the >0.1 MHz range. On the other hand, while nDEP is possible in media of higher conductivity under electric fields in the <0.1 MHz range, the degree of dielectric contrast to differentiate cells based on their DEP behavior is minimal and electrothermal flows arising from Joule heating due to electric fields within high conductivity media can lower the resolution of the separations [26, 27]. Hence, biological cells in a sample must be swapped from their culture media that typically possess conductivity levels of ~15 000 μS/cm, to the optimal media for DEP, which is at ~100-fold lower conductivity (100–500 μS/cm) and includes ingredients to reduce osmotic stress [28]. Such buffer swaps are currently performed off-chip, which requires sensitive cells to be repeatedly centrifuged, thereby requiring user intervention, and increasing the time spent by sensitive cells outside of their culture media, due to the need for time-consuming and laborious sample preparation prior to and after DEP sorting. Consequently, there have been reports on loss of cell viability post-DEP separation [29, 30], which likely occur due to the sample preparation steps, rather than due to electric field effects on cells.

Microfluidic media dilution strategies from prior reports [31, 32] are likely to also dilute cells in the sample, while inertial strategies to enhance mixing for media dilution [33] would also alter cell streamlines to cause their flow dispersion and reduce sample collection in the exchanged buffer. Other strategies for buffer exchange utilize acoustophoresis [34] or dielectrophoresis [35] for flow focusing of cells in the sample, so that the suspending media can be exchanged by cascaded ion diffusion. However, selectivity of the trapping force cannot be maintained for all cell types in heterogeneous samples, the trapping force magnitude varies as a function of exchanged media properties [36], and the increasing cell-to-cell interactions that occur during focusing of concentrated samples limit their efficacy. Also, media exchange in these prior strategies was not integrated in-line to downstream operations, such as DEP, which requires specific ranges of flow rate and media conductivity. Instead, we present a single-stage microfluidic strategy (Figure 1 and Figure S1) of small footprint (~4×2 cm) that couples flow focusing of cells at the center of a long straight channel by tangential flows, with ion diffusion at the edges, for enabling on-chip media swap of cells from their culture media to ~100-fold lower conductivity media. The hydrodynamic resistances at the outlets are adjusted to minimize flow dispersion for collecting majority of cells from the original biological sample and to modulate the flow rate of cells for enabling in-line DEP deflection downstream. Based on this, red blood cells (RBCs) in the input sample (3.3×10^8 cells/ml) are transferred from a media of 1× PBS at ~15 000 μS/cm conductivity to a buffer with a media conductivity of ~175 μS/cm and the collected sample exhibits minimal dilution (10^8 cells/ml). In this manner, the media conductivity and

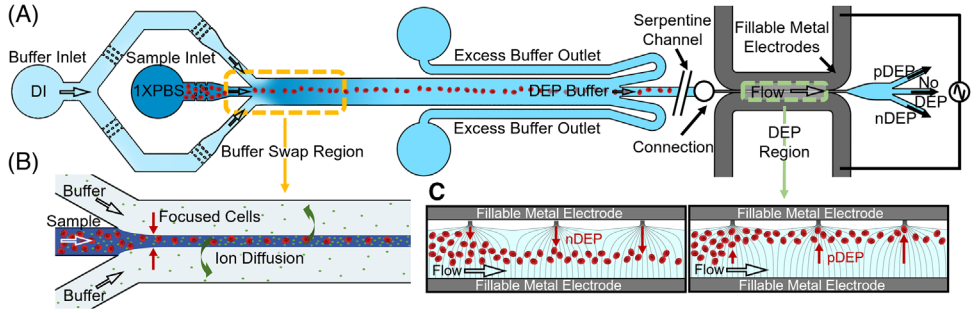

FIGURE 1 (A) Schematic of the sample buffer swap and dielectrophoretic separation stages. The central outlet from the buffer swap leads to a serpentine channel that enhances hydrodynamic resistance versus flanking outlets (see Figure S1). (B) Buffer swap occurs over the cell focusing region by ion diffusion from sample buffer to the tangential flow buffer. (C) Negative dielectrophoresis (nDEP) and positive DEP (pDEP) of the collected red blood cells (RBCs) from the buffer swap stage

flow rate of the collected sample are validated to support in-line negative dielectrophoresis (nDEP) at 30 kHz and positive dielectrophoresis (pDEP) at 1 MHz, by using a set of sequential field nonuniformities in the downstream microchannel for flowthrough DEP [37]. Based on this platform, we envision the ability for on-chip automation [38] and integration of sample preparation in-line with DEP sorting to reduce user intervention and stress on cells, as well as for monitoring of cell media properties, as well as their numbers, velocity, viability, and position in the microchannel, as may be required for tailoring DEP separations for different degrees of cellular heterogeneity within the biological sample of interest.

2 | MATERIALS AND METHODS

2.1 | Device design

A single-layer PDMS microfluidic device was designed to focus the cell streamline from the inlet via high flow rate tangential flows containing the DEP buffer. This promotes diffusion-based ion mixing across the respective flow streams of the long straight channel (2 cm in length, 1500 μm in width and 50 μm in depth) that is designed for high laminarity to minimize dispersion of cell streamlines, so that cells can be exchanged from physiological media to that of low conductivity media, as required for downstream DEP deflection (Figure 1). The collection region for cells in the swapped buffer consists of a central sample outlet, designed for a width that is larger than the flow-focused cell streamlines and for a hydrodynamic resistance that is much higher than that of the two flanking excess buffer outlets, as accomplished by the central outlet leading to a serpentine channel that is 99 times the length of the two flanking excess buffer outlets. This reduces the flow rate and flow dispersion of the cell streamlines exiting at the channel center from the buffer swap stage, while ensuring that the excess buffer is removed at high flow rate from the flanking outlets. In this manner, the cells in the sample can be collected without dilution and at modulated velocities that support downstream DEP deflection at the desired separation throughput. The enhanced net hydrodynamic resistance of the cell collection region also ensures a degree of tolerance to external flow disturbances occurring at the inlet and outlet. The collected cells in the swapped buffer pass onward to an adjoining microchannel for in-line dynamic DEP at the same flow rate, through connective tubing between the sample outlet of the buffer swap stage and the sample inlet of the DEP stage. Since the central outlet from the buffer swap region has a serpentine length (~85 cm) that is much greater than that of the DEP region (~1.5 cm), the latter region does not have a significant upstream effect on the hydrodynamic resistance balance from the buffer swap region. The media conductivity after the buffer swap stage was determined using a conductivity meter based on three independent runs for swapping cells from 1× PBS to the low conductivity buffer required for DEP.

2.2 | Device simulation

The device design and flow conditions were optimized using COMSOL Multiphysics 5.6 package. We used the microfluidics module to solve the Navier–Stokes equations for the laminar regime. We specified the volumetric flow rates of the inlets to 0.99 μl/s for the sheath flow and 0.01 μl/s for the sample. The boundary conditions of non-slip for the wall and atmospheric pressure in the outlets were applied. Concentration profiles were obtained by coupling the fluid flow module with the transport of diluted species interface to solve Fick's law diffusion equation. The initial sample concentration was set to 157 mM of Na^+ (the most abundant ion in PBS) and close to 0 (0.0001 mM) to simulate deionized water in the

sheath flows. Concentration profiles were plotted using probe lines at different locations in the device after the sheath and sample flow joined in the main channel.

2.3 | Device fabrication

The device was fabricated using standard single layer patterning of "SU-8 resist by photolithography on 4" silicon wafer to a 50 μm depth. A 5:1 PDMS base to PDMS crosslinker was used to micromold using the SU-8 pattern as a master mold. The PDMS and the SU8 master were cured at 60°C for 12 h, followed by demolding and oxygen plasma bonding of the released PDMS channel layer to a glass slide. Another PDMS channel layer with the pattern for the dynamic DEP device was fabricated in a similar manner and bonded to the same glass slide. Field's metal (RotoMetals, San Leandro, CA) was filled into the so-called electrode channels of the DEP device that adjoin the sample channel, with the device was submerged in a 65°C water bath to maintain Field's metal as a liquid. After electrode channel filling, the chip was cooled to room temperature to solidify the liquid metal and fabricate three-dimensional side wall electrodes across the sample channel for creating sequential field nonuniformities to initiate DEP.

2.4 | Microfluidic operation

RBCs from stock solution of blood type A+ human RBCs (Valley Biomedical, Winchester, VA) were suspended in RPMI 1640 HEPES (Sigma Aldrich, St. Louis, MO), supplemented with 0.5% Albumax II Lipid-Rich BSA (Sigma) and 50 mg/L hypoxanthine (Thermo Fisher Scientific) for storage and dilution, as needed. This RBC sample at a concentration level of 3.88×10^8 cells/ml in 1× PBS was swapped into a media of lower conductivity by using tangential flow of a media composed of 8% sucrose in DI water. A syringe pump and a pressure microfluidic flow controller were used to drive the sample and buffer/focus flows, respectively. A flow rate sensor coupled with the microfluidic flow controller was used to monitor the exiting sample flow rate. The sample media conductivity prior to buffer swap and after the buffer swap was measured with a conductivity meter (LAQUAtwin, Horiba) after periodic collection. An AC function generator integrated with a high-frequency amplifier was used to deliver 80 V_{pp} to the electrodes for initiating DEP over the 30 kHz to 1 MHz range [39], under dynamic flow conditions. Cell streamlines in the microchannel were imaged within the buffer swap and DEP stages of the chip using a CMOS camera connected to an inverted microscope (Zeiss Observer). The output RBC sample from the buffer swap stage was routed for in-line observation of DEP response at the same flow rate and media conductivity conditions.

3 | RESULTS

3.1 | Optimizing the mixing length for buffer swap

The chief design challenge is ensuring a sufficient mixing length for dilution of ions in the sample media to reach the media conductivity required for DEP, by diffusion of ions from sample to the adjoining tangential flows, while reducing flow dispersion of focused cells from the sample streamline into the tangential flow streamlines that lead to sample loss into the excess buffer outlet. For this purpose, computational fluid dynamic simulations of the design were performed using COMSOL to parameterize the channel geometry (length, width, and architecture) and flow rates to ensure sufficient time for ions to diffuse away from the sample media into the tangential flow streamlines, while maintaining the focused cell streamline at the channel center with minimal dispersion. The flow rate ratios (tangential to sample flow rate) and width of the buffer swap region are designed to ensure that the focused streamline just exceeds the size of individual cells in the sample. This allows the focused cell streamlines at the channel center to maintain laminarity and enhances its surface area of contact with the tangential flow to promote ion diffusion. Based on simulated concentration profiles (Figure 2A,B) and flow streamlines (Figure 2C), the equilibration of ion concentration to levels of 5 mol/m^3 is apparent over the channel width, onward from a diffusion length of 3000 μm from the sample input interface to the tangential flow. Table 1 summarizes the flow rate, and the sample media conditions prior to and after the buffer swap stage. Based on this, the media conductivity level prior to the buffer swap stage of: 14 150 ± 21 μS/cm (three independent measurements) can be diluted ~100-fold after the buffer swap stage to: 173.3 ± 1.7 μS/cm (three independent measurements), using ~200-fold higher flow rate for the sheathing flow (~129 μl/min) versus the sample flow (0.6 μl/min). The resulting outlet from the buffer swap stage is optimized for minimal loss of cells (~10^8 cell/ml in collected sample) and has a flow rate of 1.8 μl/min, which will be validated subsequently for their DEP behavior.

3.2 | Optimizing outlet hydrodynamic resistance for reducing sample loss

Flow dispersion of the focused cell streamline over this minimum required mixing length was simulated using the particle tracing module, so that the flow conditions can be

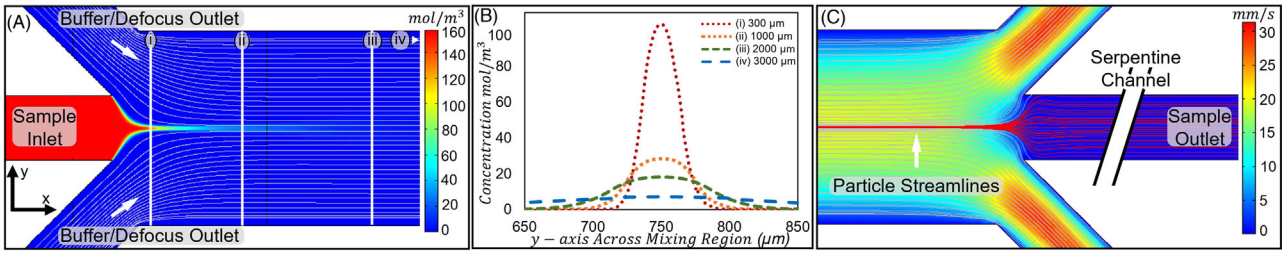

FIGURE 2 Simulations of the buffer swap stage to show (A) ion concentration profiles due to diffusion from sample media to tangential flow media. (B) ion concentration profiles across width of the microchannel along progressive mixing lengths from sample inlet: (i) 300 µm, (ii) 1000 µm, (iii) 2000 µm, and (iv) 3000 µm, per lines in (A). (C) Streamlines for cells (red) and buffer (shaded) show differences in flow velocity of the central versus flanking outlets from the buffer swap stage, due to the excess hydrodynamic resistance from the serpentine channel after the central outlet

TABLE 1 Flow rate and media conductivity at the inlet and outlet of the buffer swap stage. The last row of the buffer conductivity is the average and standard deviation of $n = 3$ measurements

Flow rate (µl/min)			Buffer conductivity (µS/cm)	
Sample inlet	Sheath inlet	Sample outlet	Initial	Final
0.6	129	1.8	14 150	173
0.6	130.2	1.8	14 180	177
0.6	130.2	1.8	14 130	176
Collected sample ~10^8 cells/ml			Mean + SD ($n = 3$) 14 153 ± 21	175.3 ± 1.7

optimized to enable ion diffusion, while maintaining a low Stokes number (<0.1) to ensure that the particles follow their flow streamlines (Figure 2C). To ensure that the cells follow the streamline toward the central collection outlet rather than exhibiting deviation into the flanking outlets that are designed for collection of excess buffers, the width and hydrodynamic resistances for each outlet branch were modulated. The width of the central outlet is designed to be much larger than that of the focused cell streamlines (Figure 2C) to slow the flow rate of cells after their speeding under tangential flow, and to maximize their collection. Furthermore, the outlet from the central collection region leads to a serpentine channel of 99 times greater length versus that of the flanking channels, thereby vastly increasing the hydrodynamic resistance of the central outlet versus the flanking channels. Hence, the net flow rate of the focused cell streamline is reduced at the outlet, while excess buffer from ion diffusion to cause the media conductivity alteration can be removed at high flow rate through the flanking channels (see flow velocity profiles of central and flanking outlets in Figure 2C). As a result, the cell streamline passes with minimal flow dispersion for collection at the central outlet at a modulated flow rate (only threefold higher than input sample flow rate) that supports dielectrophoretic deflection. Results from hemocytometer runs on regularly drawn samples (Table 1) confirm collection of a majority of cells from the input sample, with the dead volume of the connective tubing between the buffer swap and DEP regions responsible for much of the sample loss. The device overview (Figure 3A) shows that the focused cells entering the buffer swap region (Figure 3(i)) retain their focus across the mixing length to enter the central collection channel (Figure 3(ii)) with minimal cell loss due to flow defocusing (see Supporting Information Video S1).

3.3 | Validation for in-line dielectrophoretic deflection

Based on this optimized design for the buffer swap, the measured outlet flow rates (~1.8 µl/min) and diluted media conductivities (~175 µS/cm) (Table 1) are validated to establish the ability to cause in-line dielectrophoresis, as per the flow schematic of the device (Figure 4A) and images of the field nonuniformity (Figure 4B) and 3D structure of the electrode interface with the sample channel (Figure 4C).

Details on the pDEP and nDEP deflection are in Supporting Information Videos S2 S3, respectively (also Section S5). As per the comparison before (Figure 5A) and after the electric field at 30 kHz (Figure 5B), nDEP is apparent based on translation of the cell streamline away from the high field region (see arrows in Figure 5B). Similarly, after the electric field at 1 MHz (Figure 5C), pDEP is apparent based on translation of the cell streamline toward the high-field region (see arrows). It is noteworthy that the current device lacks a tangential flow after the buffer swap stage to focus the cells with respect to the field nonuniformity for enabling sequential DEP deflection. Hence, the nDEP and pDEP deflection are not as clearly apparent as in our prior work [37] that used focusing flows, but lacked the buffer swap stage. Nevertheless, based on crossover frequency measurements on RBCs after the reported on-chip buffer swap, we confirm that

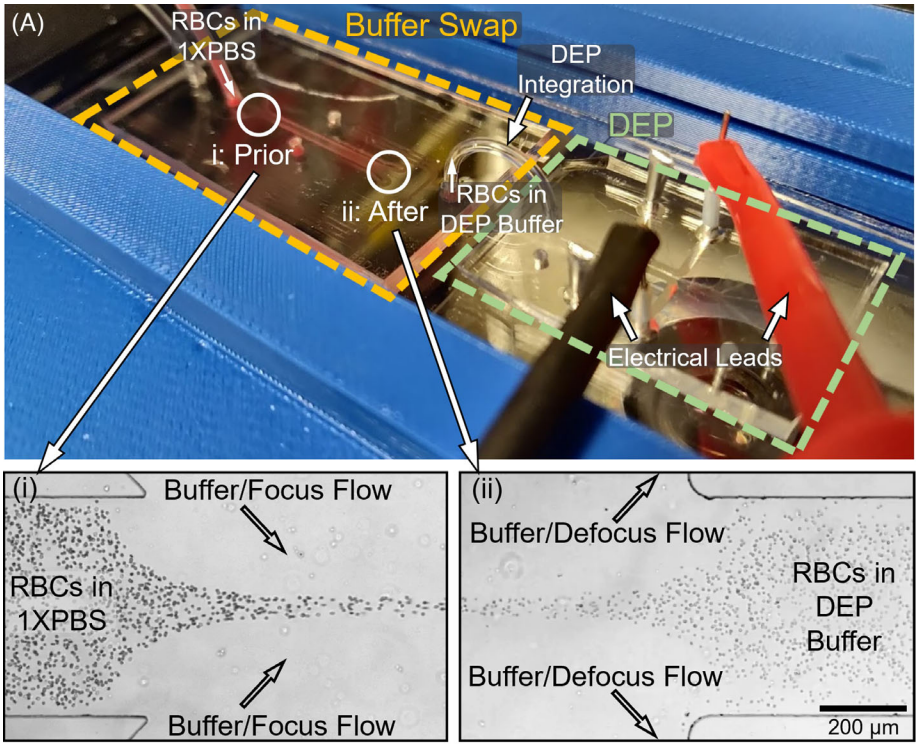

FIGURE 3 (A) Setup for the buffer swap stage connected to the dielectrophoresis (DEP) stage. Microscope images of (i) red blood cells (RBCs) suspended in 1× PBS (14 150 µS/cm) entering the buffer swap region at 0.6 µl/min and (ii) exiting as RBCs in the swapped buffer (173 µS/cm) at 1.8 µl/min

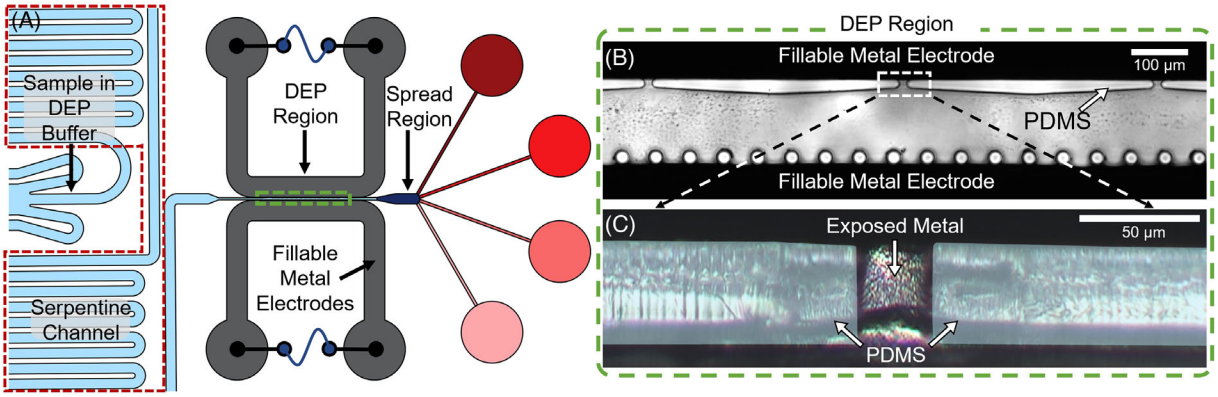

FIGURE 4 (A) Connection from buffer swap region to the dielectrophoresis (DEP) device region through serpentine channel to modulate hydrodynamic resistance (also see Figure S1). (B) Sequential field nonuniformities due to electrodes architecture across sample channel. (C) Expanded view of the orifice region (dashed white box) showing the 3D electrode interface in the sample channel

the computed membrane capacitance of 11.25 mF/m^2 (see Supporting Information S5 and S6) is close to that of prior work [40].

4 | CONCLUDING REMARKS

To address the need for swapping biological cells from their culture media into a media with a conductivity level that is optimized for dielectrophoretic manipulation and vice versa post-dielectrophoretic separation, we present a microfluidic device with a buffer swap stage that is connected in-line to a dielectrophoretic stage. The microfluidic design and flow conditions were optimized using flow and particle tracing simulations for enabling ion diffusion from sample stream into tangential flows, while appropriately increasing the hydrodynamic resistance of the outlet collection channel versus that

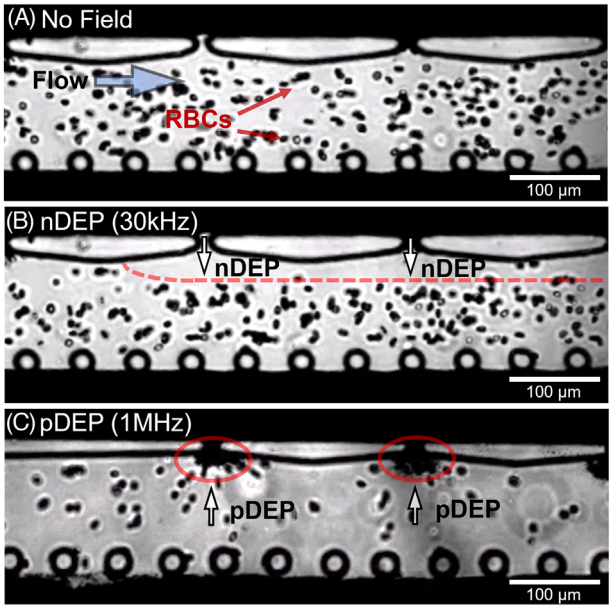

FIGURE 5 Downstream flowthrough dielectrophoresis (DEP) of red blood cells after outflow from the buffer swap stage at 1.8 µl/min in media of ~175 µS/cm conductivity for deflection per streamlines in Figure 1C. (A) Initial streamline of dispersed red blood cells (RBCs) prior to DEP deflection. (B) nDEP at 30 kHz for translation away from the high field region (see arrows). (C) pDEP at 1 MHz for translation toward the high field region (see arrows). See Supporting Information Videos S2 and S3, respectively

of the flanking excess buffer outlet channels, thereby minimizing the flow dispersion of cells to enhance their collection and to modulate their flow rate for supporting downstream DEP. As a result, RBCs entering the buffer swap stage at of 3.88×10^8 cells/ml at 0.6 µl/min in 1× PBS media (14 150 µS/cm) can be diluted ~100-fold in media conductivity after the buffer swap stage (~175 µS/cm), using ~200-fold higher flow rate for the sheathing flow (~129 µl/min) versus the sample flow. The sample outlet from the buffer swap stage with ~10^8 cells/ml has a media conductivity of ~175 µS/cm and a flow rate of 1.8 µl/min, which is validated in-line for downstream nDEP at 30 kHz and pDEP at 1 MHz. Follow-up work will integrate the buffer swap stage on a single chip, prior to and after DEP, and include in-line monitoring to characterize the outlet sample media conductivity, cell numbers, cell velocity, cell viability, and the position of cell streamlines for tailoring the sample toward effective DEP separations.

ACKNOWLEDGMENTS

Funding from NSF Award #2051652, AFOSR contract FA2386-21-1-4070, NCI Cancer Center Support Grant P30 CA44579, and from CytoRecovery, Inc. are acknowledged. Technical discussions with Rafael Davalos (Virginia Tech) and Alexandra Hyler (CytoRecovery, Inc.) on relevant sample types and device integration steps are acknowledged.

CONFLICT OF INTEREST

The authors have declared no conflict of interest.

DATA AVAILABILITY STATEMENT

The data that support the findings of this study are available in the Supporting Information section and from the corresponding author upon reasonable request.

ORCID

Karina Torres-Castro https://orcid.org/0000-0001-9959-6040
Nathan S. Swami https://orcid.org/0000-0002-0492-1160

REFERENCES

1. Perkins TJ, Swain PS. Strategies for cellular decision-making. Mol Syst Biol. 2009;5:326.
2. Cros J, Raffenne J, Couvelard A, Poté N. Tumor heterogeneity in pancreatic adenocarcinoma. Pathobiology 2018;85:64–71.
3. Wlodkowic D, Skommer J, Darzynkiewicz Z. Cytometry in cell necrobiology revisited. Recent advances and new vistas. Cytometry A. 2010;77:591–606.
4. Grützkau A, Radbruch A. Small but mighty: how the MACS-technology based on nanosized superparamagnetic particles has helped to analyze the immune system within the last 20 years. Cytometry A. 2010;77:643–7.
5. Mcgrath JS, Honrado C, Moore JH, Adair SJ, Varhue WB, Salahi A, et al. Electrophysiology-based stratification of pancreatic tumorigenicity by label-free single-cell impedance cytometry. Anal Chim Acta. 2020;1101:90–8.
6. Yale AR, Nourse JL, Lee KR, Ahmed SN, Arulmoli J, Jiang AYL, et al. Cell surface N-glycans influence electrophysiological properties and fate potential of neural stem cells. Stem Cell Rep. 2018;11:869–82.
7. Petchakup C, Tay HM, Li KHoH, Hou HW. Integrated inertial-impedance cytometry for rapid label-free leukocyte isolation and profiling of neutrophil extracellular traps (NETs). Lab Chip. 2019;19:1736–46.
8. Zhou J, Mukherjee P, Gao H, Luan Q, Papautsky I. Label-free microfluidic sorting of microparticles. APL Bioeng. 2019;3:041504.
9. Luan Q, Macaraniag C, Zhou J, Papautsky I. Microfluidic systems for hydrodynamic trapping of cells and clusters. Biomicrofluidics 2020;14:031502.
10. Honrado C, Adair SJ, Moore JH, Salahi A, Bauer TW, Swami NS. Apoptotic bodies in the pancreatic tumor cell culture media enable label-free drug sensitivity assessment by impedance cytometry. Adv Biol. 2021;5:2100438.
11. Varhue WB, Langman L, Kelly-Goss M, Lataillade M, Brayman KL, Peirce-Cottler S, et al. Deformability-based microfluidic separation of pancreatic islets from exocrine acinar tissue for transplant applications. Lab Chip. 2017;17:3682–91.
12. Rohani A, Moore JH, Su Y-H, Stagnaro V, Warren C, Swami NS. Single-cell electro-phenotyping for rapid assessment of

Clostridium difficile heterogeneity under vancomycin treatment at sub-MIC (minimum inhibitory concentration) levels. Sens Actuators B. 2018;276:472–80.
13. Pohl HA. The motion and precipitation of suspensoids in divergent electric fields. J Appl Phys. 1951;22:869–71.
14. Pethig R, Menachery A, Pells S, De Sousa P. Dielectrophoresis: A review of applications for stem cell research. Biomed Res Int. 2010;2010:182581.
15. Morgan H, Green NG. AC electrokinetics: colloids and nanoparticles. Philadelphia: Research Studies Press; 2003.
16. Gagnon ZR. Cellular dielectrophoresis: applications to the characterization, manipulation, separation and patterning of cells. Electrophoresis 2011;32:2466–87.
17. Torres-Castro K, Honrado C, Varhue WB, Farmehini V, Swami NS. High-throughput dynamical analysis of dielectrophoretic frequency dispersion of single cells based on deflected flow streamlines. Anal Bioanal Chem. 2020;412:3847–57.
18. Gascoyne P, Shim S. Isolation of circulating tumor cells by dielectrophoresis. Cancers 2014;6:545–79.
19. Li M, Anand RK. High-throughput selective capture of single circulating tumor cells by dielectrophoresis at a wireless electrode array. J Am Chem Soc. 2017;139:8950–9.
20. Adams TNG, Jiang AYL, Mendoza NS, Ro CC, Lee D-H, Lee AP, et al. Label-free enrichment of fate-biased human neural stem and progenitor cells. Biosens Bioelectron. 2020;152:111982.
21. Rohani A, Moore JH, Kashatus JA, Sesaki H, Kashatus DF, Swami NS. Label-free quantification of intracellular mitochondrial dynamics using dielectrophoresis. Anal Chem. 2017;89:5757–64.
22. Su Y-H, Warren CA, Guerrant RL, Swami NS. Dielectrophoretic monitoring and interstrain separation of intact clostridium difficile based on their S(surface)-layers. Anal Chem. 2014;86:10855–63.
23. Liu Y, Hayes MA. Differential biophysical behaviors of closely related strains of salmonella. Front Microbiol. 2020;11:302.
24. Shi L, Kuhnell D, Borra VJ, Langevin SM, Nakamura T, Esfandiari L. Rapid and label-free isolation of small extracellular vesicles from biofluids utilizing a novel insulator based dielectrophoretic device Lab Chip. 2019;19:3726–34.
25. Moore JH, Varhue WB, Su Yi-H, Linton SS, Farmehini V, Fox TE, et al. Conductance-based biophysical distinction and microfluidic enrichment of nanovesicles derived from pancreatic tumor cells of varying invasiveness. Anal Chem. 2019;91:10424–31.
26. Chaurey V, Rohani A, Su Y-H, Liao K-T, Chou C-F, Swami NS. Scaling down constriction-based (electrodeless) dielectrophoresis devices for trapping nanoscale bioparticles in physiological media of high-conductivity Electrophoresis 2013;34:1097–104.
27. Chaurey V, Polanco C, Chou C-F, Swami NS. Floating-electrode enhanced constriction dielectrophoresis for biomolecular trapping in physiological media of high conductivity. Biomicrofluidics 2012;6:012806.
28. Hyler AR, Hong D, Davalos RV, Swami NS, Schmelz EM. A novel ultralow conductivity electromanipulation buffer improves cell viability and enhances dielectrophoretic consistency. Electrophoresis 2021;42:1366–77.
29. Mittal N, Rosenthal A, Voldman J. nDEP microwells for single-cell patterning in physiological media. Lab Chip. 2007;7:1146–53.
30. Lu J, Barrios CA, Dickson AR, Nourse JL, Lee AP, Flanagan LA. Advancing practical usage of microtechnology: a study of the functional consequences of dielectrophoresis on neural stem cells Integr Biol. 2012;4:1223–36.
31. Teerapanich P, Pugnière M, Henriquet C, Lin Y-L, Naillon A, Joseph P, et al. Nanofluidic fluorescence microscopy with integrated concentration gradient generation for one-shot parallel kinetic assays. Sens Actuators B. 2018;274:338–42.
32. Wan H, Yin H. Tunable and quantitative serial dilution on multi-channel miniaturized microfluidic electrochemical platform. Sens Actuators B. 2018;274:682–8.
33. Gossett DR, Tse HTK, Dudani JS, Goda K, Woods TA, Graves SW, et al. Inertial manipulation and transfer of microparticles across laminar fluid streams Small 2012;8:2757–64.
34. Augustsson P, Åberg LB, Swärd-Nilsson A-MK, Laurell T. Buffer medium exchange in continuous cell and particle streams using ultrasonic standing wave focusing Microchim Acta. 2009;164:269–77.
35. Ma Z, Zhao H, Shi L, Yu D, Guo X. Automatic medium exchange for micro-volume cell samples based on dielectrophoresis. Electrophoresis 2021;42:1507–15.
36. Farmehini V, Kiendzior S, Landers JP, Swami NS. Real-time detection and control of microchannel resonance frequency in acoustic trapping systems by monitoring amplifier supply currents. ACS Sens. 2021;6:3765–72.
37. Huang X, Torres-Castro K, Varhue W, Salahi A, Rasin A, Honrado C, et al. Self-aligned sequential lateral field non-uniformities over channel depth for high throughput dielectrophoretic cell deflection. Lab Chip. 2021;21:835–43.
38. Farmehini V, Varhue W, Salahi A, Hyler AR, Cemazar J, Davalos RV, et al. On-chip impedance for quantifying parasitic voltages during AC electrokinetic trapping. IEEE Trans Biomed Eng. 2019;67:1664–71.
39. Farmehini V, Rohani A, Su Y-H, Swami NS. A wide-bandwidth power amplifier for frequency-selective insulator-based dielectrophoresis. Lab Chip. 2014;14:4183–7.
40. Wang X-Bo, Yang J, Huang Y, Vykoukal J, Becker FF, Gascoyne PRC. Cell separation by dielectrophoretic field-flow-fractionation. Anal Chem. 2000;72:832–9.

SUPPORTING INFORMATION

Additional supporting information may be found in the online version of the article at the publisher's website.

How to cite this article: Huang X, Torres-Castro K, Varhue W, Rane A, Rasin A, Swami NS. On-chip microfluidic buffer swap of biological samples in-line with downstream dielectrophoresis. Electrophoresis 2022;43:1275–1282. https://doi.org/10.1002/elps.202100304